Liquid Crystals
Publication details, including instructions for authors and subscription information:
http://www.informaworld.com/smpp/title~content=t713926090

The structure of intermediate ribbon phases in surfactant systems

H. Hagslätt[a]; O. Söderman[a]; B. Jönsson[a]
[a] Department of Physical Chemistry 1, Chemical Center, University of Lund, Lund, Sweden

To cite this Article Hagslätt, H. , Söderman, O. and Jönsson, B.(1992) 'The structure of intermediate ribbon phases in surfactant systems', Liquid Crystals, 12: 4, 667 — 688
To link to this Article: DOI: 10.1080/02678299208029102
URL: http://dx.doi.org/10.1080/02678299208029102

LIQUID CRYSTALS, 1992, VOL. 12, NO. 4, 667–688

The structure of intermediate ribbon phases in surfactant systems

by H. HAGSLÄTT*, O. SÖDERMAN and B. JÖNSSON

Department of Physical Chemistry 1, Chemical Center, University of Lund, P.O.B. 124, S-221 00 Lund, Sweden

(*Received 2 March 1992; accepted 18 April 1992*)

Intermediate phases consisting of elongated rods with a non-circular cross section (i.e. ribbons) that pack on a deformed hexagonal lattice are often formed in surfactant systems. The crystallographic lattice of such a ribbon phase can be either of oblique (or two dimensional monoclinic), primitive rectangular, centred rectangular or hexagonal symmetry, all of which are observed according to the literature. We have studied a ribbon phase that is formed in the dodecyl-1,3-propylene-bisamine/HCl/water system, by means of SAXS experiments, and a centred rectangular structure is obtained. In addition, we have reviewed, and partially reinterpreted, previously published results on the structure of different ribbon phases. 21 scattering data sets for ribbon phases of lower than hexagonal symmetry have been analysed. Both the centred rectangular (cmm) and the primitive rectangular (pmm) symmetry fit 10 of the data sets, whereas only a centred rectangular lattice can be fitted to the other 11 data sets. There is no experimental indication that supports the existence of an oblique ribbon (p2) phase. The underlying physical reasons for the observation that the centred rectangular structure is favoured are discussed in terms of a cell model approach. The energetically most favoured cell model has a centred rectangular symmetry (cmm), in accord with the experimental data, and is termed the hexagon-rod model. This model can be used to evaluate the dimensions of the deformed rods of the centred rectangular ribbon phase from scattering data and NMR data separately. One major advantage of the hexagon-rod model is that the smallest dimension of the aggregate is not required as an input parameter in the calculations. Axial ratios between 1·2 : 1 : 1–2 : 1 for the aggregates are obtained when this model is applied to SAXS, SANS and NMR data for the centred rectangular ribbon phase for none different systems.

1. Introduction

The normal hexagonal phase in surfactant systems consists of long cylinders of amphiphiles that are packed with a hexagonal symmetry [1, 2]. At higher surfactant volume fractions a lamellar phase is often found in ionic surfactant systems [2, 3]. Phases of these two symmetries have been extensively studied over the years and it is fair to state that we now have a good understanding of them [2, 4]. However, several different phases are found at surfactant concentrations between those where the hexagonal and the lamellar phases are found [5–11], and presently there is a major interest in the study of these. A collective name for these phases is, due to their location in the phase diagrams, intermediate phases [5, 6]. The hexagonal rods can change shape in that their circular cross-sections are deformed to a more or less elliptical shape [5–8, 12], and the resulting aggregates are often termed ribbons [13]. The corresponding phases are commonly called ribbon phases, and they are the intermediate phases

* Author for correspondence.

0267–8292/92 $3·00

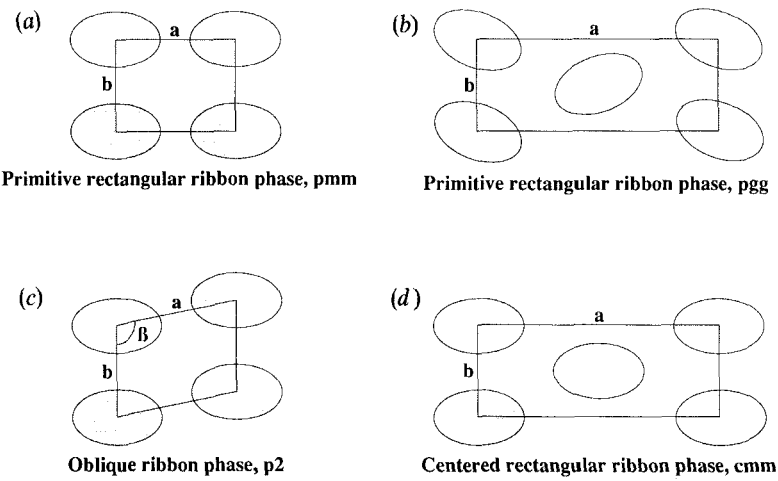

Figure 1. Proposed structures for the ribbon phases of the two dimensional space groups: (*a*) pmm, (*b*) pgg, (*c*) p2 and (*d*) cmm, where *a*, *b* and β are unit cell dimensions and angle, respectively.

that appear closest to the normal hexagonal phase [5–8]. Other intermediate phases are the rhombohedral phase [9], different bicontinuous cubic phases [10] and the tetragonal phase [9, 11, 14]. This work is concerned only with the ribbon phases. The first evidence for the existence of a ribbon phase was obtained by Luzzati and co-workers in 1960 [5, 6]. A phase with a primitive rectangular symmetry, as determined by small angle X-ray scattering (SAXS) measurements, was found in four different binary surfactant/water systems, viz. potassium oleate, sodium oleate, potassium palmitate and potassium laurate. It was suggested that the phase consisted of elongated aggregates with elliptic-like cross-sections packed on a lattice with the two dimensional space group pmm (see figure 1 (*a*)). Later on, Hendrikx and Charvolin [7] performed SAXS measurements on the sodium decyl sulphate/1-decanol/water system and obtained data that could be indexed on a centred rectangular lattice, and suggested the space group cmm (see figure 1 (*d*)).

The first direct proof in favour of the ribbon-like shape of the aggregates were reported by Chidichimo *et al.* [12], in the three component systems potassium palmitate/potassium laurate/water and sodium decyl sulphate/1-decanol/water. With ^{2}H NMR measurements on D_2O and potassium palmitate-d_3, powder patterns having non-zero asymmetry parameters were obtained for the intermediate phase [12, 15]. This observation was interpreted in terms of a phase consisting of ribbon-like aggregates [12]. Alpérine *et al.* [16] showed by small angle neutron scattering (SANS) that sodium decyl sulphate and 1-decanol (in the ternary system with water) are not uniformly distributed within the deformed elongated rods of the centred rectangular phase. The decanol content is higher at the central parts of the aggregates, than at the more curved edges. In 1987, Hendrikx and Charvolin [8] published evidence for a non-rectangular packing of ribbon-shaped elongated aggregates. Neutron scattering experiments indicated that a part of the hexagonal phase of the sodium decyl sulphate/1-decanol/water system consists of deformed aggregates.

An oblique (or two dimensional monoclinic) packing of the ribbons has been proposed as well (see figure 1 (*c*)), for the sodium dodecyl sulphate/water system [9, 17].

However, on the basis of SAXS measurements on this system, Auvray *et al.* [18] have recently proposed a centred rectangular symmetry for the ribbon phase. In the hexadecyltrimethylammonium bromide (CTAB)/water system Auvray *et al.* fitted both an oblique lattice and a centred rectangular lattice to the obtained SAXS data [19]. An oblique phase with circular cylinders has also been proposed [20, 21].

It is the aim of this paper to discuss the experimental evidence concerning the different structures of the ribbon phases, and to discuss their formation from a thermodynamic point of view. To this end we have studied the dodecyl-1,3-propylene-bisamine/HCl/water system, where an intermediate ribbon phase is found. The impetus for studying this system is the fact that the average charge of the surfactant can be varied from 0 to +2, thus providing means to investigate the influence which the surfactant charge has on the properties of surfactant systems. The investigations are based on SAXS measurements on the ribbon phase in this system, but also on previously published SAXS, SANS and NMR data on ribbon phases. Some of these data will be partially reinterpreted.

2. Experimental

2.1. *Materials*

Dodecyl-1,3-propylene-bisamine (DoPDA), CH_3–$(CH_2)_{11}$–NH–$(CH_2)_3$–NH_2, was obtained from Berol Nobel, Sweden. The diamine surfactant has a purity better than 97 per cent, as checked by gas liquid chromatography and ^{13}C NMR, the rest mainly containing diamines with somewhat shorter or longer alkyl chains. The dihydrochloride form was prepared by adding a solution of the diamine in ethanol to a surplus of HCl, also dissolved in ethanol. The precipitated dodecyl-1,3-propylene-bisammoniumchloride (DoPDAC) crystals were washed with water and used without further purification. The chloride content in the DoPDAC was determined by elementary analysis to be 22·5 wt%, which is equal to the theoretical value. DoPDA and HCl, with a 1 : 1 molar ratio, were dissolved in water and the solution was freeze dried in order to yield the mono-hydrochloride of the alkyl diamine. A chloride content of 13·0 wt% was obtained for this compound, corresponding to 1·02 HCl molecules per surfactant molecule. By using appropriate mixtures of the three alkyl diamines with different hydrochloride contents the three component system DoPDA/HCl/water can be conveniently investigated. For simplicity we name the resulting diamines (DA) by their hydrochloride content, $z(0 \leqslant z \leqslant 2)$, for example dodecyl-1,3-propylene-bisammoniumchloride (DoPDAC) will be referred to as DA + 2.

The densities of DA + 2 and DA + 1·02 were measured by an Anton Paar Density Meter DMA 46 to be 1·018 g cm^{-3} and 0·9536 g cm^{-3}, respectively, in the concentration range of 0–15 wt%, corresponding to surfactant volumes, V_s, of 514·4 Å^3 and 487·3 Å^3 for the two cases. We have assumed the surfactant volume to be a linear function of the hydrochloride content, and thus $V_s(z)/\text{Å}^3 = 458{\cdot}8 + 27{\cdot}74z$.

2.2. *Phase diagram*

Samples were prepared by adding the components directly to glass tubes that were then flame sealed and homogenized by repeated heating and centrifugation back and forth. The samples were then equilibrated for at least one month at room temperature before being investigated by means of optical microscopy, ^2H NMR measurements on heavy water and X-ray measurements.

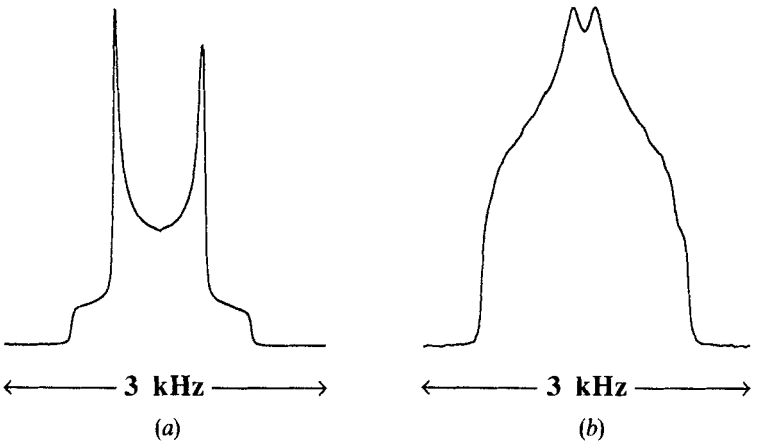

Figure 2. ^{2}H NMR spectra from heavy water obtained from (*a*) the hexagonal phase ($\eta = 0$) and (*b*) the centred rectangular phase ($\eta \neq 0$) in the dodecyl-1,3-propylene-bisamine/HCl/D_2O system at 25°C. The composition of the samples are DA + 1·02/50 per cent and DA + 1·02/54 per cent, respectively.

2.3. *^{2}H NMR measurements*

The ^{2}H NMR measurements of heavy water were performed on a Bruker MSL-100 spectrometer operating at 15·371 MHz. The ^{2}H NMR method is an important tool in the determination of phase diagrams in surfactant systems [22], since the quadrupolar spectra (cf. figure 2) are in general different for different phases [22]. This follows since the bandshape of the spectra reflects the structure of the hydrophilic/hydrophobic interface. For phases, where the aggregates have an axis of symmetry with an order less than three, spectra with an asymmetry parameter (η) not equal to zero are obtained [12, 15]. An example of the latter case from the system presently under study is given in figure 2 (*b*). For multi-phase samples, the spectra are simply the sum of the individual spectra for each phase weighted by their fraction of the sample.

2.4. *Small angle X-ray scattering (SAXS)*

To identify the different phases we have performed small angle X-ray scattering measurements at 25°C with a camera with pin hole collimation after Kiessig [23, 24] and copper K_α radiation that was nickel filtered. The sample to film distance was 0·2085 m. When evaluating the diffractograms, the values of the Miller indices for the appropriate space group were first assigned to the Bragg spacings obtained from the films. Subsequently, the best values of the unit cell dimensions were obtained by minimizing the sum of the squared differences between the observed and calculated Bragg spacings.

3. Results and discussion

3.1. *Nomenclature*

The symmetry of a phase is not uniquely determined by the structure of its aggregates. For example, prolate micelles can form cubic [10, 25, 16] and nematic phases [27], in addition to a micellar solution phase [28]. Conversely, from the symmetry of the phase alone, little can be said about the aggregation structure. This is seen for example, for the cubic phases, which can be either bicontinuous of several different space groups [10], or discontinuous (packed micelles) [10, 26]. For cases,

where the symmetry of the phase and the structure of the aggregates are both known, it is preferable that the name given to the phase reflects this fact. Thus, when it is possible, we name the ribbon phases of different symmetry according to this principle.

3.2. *The ribbon phase of the dodecyl-1,3-propylene-bisamine/HCl/water system*

In order to determine the phase diagram for the DoPDA/HCl/water system, samples were prepared with ordinary water replaced with heavy water, and subsequently the ^{2}H NMR spectra were recorded in order to determine the phase boundaries. With this method, an intermediate phase with ribbon-like aggregates was found in this system and for which powder patterns with $\eta \neq 0$ were obtained (see figure 2 (*b*)). The intermediate phase (the compositions of the samples studied in the present work are given in table 2) is, by two-phase regions, in equilibrium with a lamellar phase at higher surfactant concentrations and with a hexagonal phase at lower surfactant concentrations. These three phases were investigated by means of SAXS measurements of single phase samples, as evidenced by their ^{2}H NMR spectra. In this paper we give the results for the intermediate phase, whereas the other results will be reported on in a future paper which treats the phase diagram of the DoPDA/HCl/water system more extensively [29].

Four samples of different compositions in the intermediate phase were investigated by means of X-ray scattering, and in all cases the data could be indexed to a rectangular space group. For a two dimensional rectangular symmetry, the Bragg spacings are calculated from [30]

$$d_{hk} = \left(\frac{h^2}{a^2} + \frac{k^2}{b^2}\right)^{-1/2}, \tag{1}$$

where h and k are the Miller indices for the plane. For the centred symmetry (cmm), the restriction $h+k=2n$, where n is an integer, has to be fulfilled, whereas there is no restriction for h and k for the primitive structure of space group pmm. In the case of the primitive rectangular lattice of space group pgg the restriction is that $h+k=2n$ for $h=0$ or $k=0$. The unit cell dimensions, a and b, are defined as in figure 1. Both primitive (pmm) and centred rectangular lattices could be fitted to one of the data sets, whereas only a centred rectangular lattice would seem to fit the other three data sets (see table 2). An example is given in table 3, where it can be seen that the centred rectangular space group gives a better fit to the data than the primitive rectangular (pmm) one.

Table 1. List of abbreviations for surfactants and cosurfactants.

NaO	Sodium oleate
KO	Potassium oleate
KP	Potassium palmitate
KL	Potassium laurate
SDS	Sodium dodecyl sulphate
SdS	Sodium decyl sulphate
CTAB	Hexadecyltrimethylammonium bromide
CTAC	Hexadecyltrimethylammonium chloride
DoTAC	Dodecyltrimethylammonium chloride
DoPDA	Dodecyl-1,3-propylene-bisamine (DA + 0)
DoPDAC	Dodecyl-1,3-propylene-bisammoniumchloride (DA + 2)
DA + z	Dodecyl-1,3-propylene-bisamine + z HCl, $0 \leqslant z \leqslant 2$
dec	1-Decanol

Table 2. Evaluation of SAXS data from different ribbon phases. n_B is the number of obtained Bragg reflections and Sym is the structure proposed from evaluation of the SAXS data, and a and b are the unit cell dimensions. Other notation is as defined in the text.

System	T/°C (*a*)	C_s/% (*a*)	C_c/% (*a*)	C_w/% (*a*)	n_B (*a*)	Sym (*a*)	Sym (*b*)	a/Å (*c*)	b/Å (*c*)	ϕ_{hc} (*d*)	r_s/Å (*e*)	d_w/Å (*e*)	ρ (*e*)
NaO/H_2O [5,6]	65	56		44	2	pmm	cmm, pmm	91·2	42·1	0·535	14·8	6·3	1·31
KO/H_2O [5,6]	20	64		36	4	pmm	cmm, pmm	107·8	45·5	0·583	16·6	6·2	1·44
KO/H_2O [31]	20	60		40	2	pmm	cmm, pmm	110·0	48·0	0·548	16·9	7·1	1·40
KO/H_2O [31]	20	62·9		37·1	4	pmm	cmm, pmm	111·8	47·1	0·573	17·0	6·6	1·45
KO/H_2O [31]	20	65·5		34·5	2	pmm	cmm, pmm	110·0	47·8	0·596	17·7	6·2	1·38
KP/H_2O [5,6]	70	60		40	2	pmm	cmm, pmm	103·4	44·5	0·532	15·4	6·9	1·43
KP/H_2O [45]	59	59		41	4	pmm	cmm, pmm	112·8	42·0	0·522	14·0	7·0	1·72
KP/H_2O [45]	75	59		41	4	pmm	cmm, pmm	108·8	42·3	0·524	14·2	6·9	1·62
$CTAB/H_2O$ [19]	40·5	≈80		≈20	8	p2, cmm	cmm	95·2	43·4	0·612	16·4	5·3	1·30
$DA+0·81/D_2O$	25	50·5		49·5	2		cmm, pmm	116·9	45·7	0·398	19·9	9·9	1·73
$DA+1·02/D_2O$	25	54·0		46·0	4		cmm	113·4	46·2	0·415	13·6	9·6	1·62
$DA+1·02/D_2O$	25	58·2		41·8	4		cmm	115·9	44·2	0·445	13·3	8·8	1·74
$DA+1·11/D_2O$	25	60·0		40·0	4		cmm	111·8	43·8	0·454	13·5	8·4	1·67
$DoTAC/H_2O$ [32]	24	81·6		18·4	4	cmm	cmm	84·9	36·9	0·590	13·6	4·9	1·39
SDS/D_2O* [43]	55	58·5		41·5	3	p2	cmm	94·8	40·9	0·484	13·4	7·1	1·45
SDS/D_2O [9]	55	60		40	7	p2	cmm	89·0	39·3	0·496	13·1	6·6	1·40
SDS/H_2O [18]	37	≈60		≈40	10	cmm	cmm	89·2	40·0	0·475	13·0	7·0	1·38
SDS/H_2O [18]	46·5	≈60		≈40	5	cmm	cmm	99·6	36·8	0·476	11·5	6·9	1·78
SDS/H_2O [18]	47·2	≈60		≈40	?	cmm	?	102·6 (*a*)	36·8 (*a*)	0·474	11·4	7·0	1·85
KL/H_2O [5,6]	20	61		39	2	pmm	cmm, pmm	95·0	35·8	0·506	11·7	6·2	1·70
$SdS/dec/H_2O$ [7]	22	47·2	5·2	47·6	4	cmm	cmm	99·4	38·0	0·408	10·8	8·2	1·78
$SdS/dec/H_2O$ [16]	23	46·1	6·3	47·6	?	pgg	?	106·0 (*a*)	38·0 (*a*)	0·412	10·7	8·3	1·94

*SANS data.
(*a*) Data taken from the references.
(*b*) Results from calculations in this work.
(*c*) A centred rectangular symmetry is assumed.
(*d*) Calculated according to equation (3) with group volumes from table 6. The water volumes are taken from [46].
(*e*) Calculated with the hexagon-rod model.

Table 3. Observed Bragg spacings (d_{obs}) at 25°C, and results for the best pmm (d_p) and cmm (d_c) fits to the data. For the centred rectangular fit the cell dimensions are $a = 111{\cdot}8$ Å and $b = 43{\cdot}8$ Å, whereas $a = 55{\cdot}7$ Å and $b = 40{\cdot}5$ Å for the primitive rectangular fit. The sample consists of 60·0 wt% of DA + 1·11 in D_2O. The uncertainties are estimated from the width of the reflections.

hk_p	d_p/Å	d_{obs}/Å	d_c/Å	hk_c
1 0	55·7	55·9 ± 0·5	55·9	2 0
0 1	40·5	40·7 ± 0·4	40·8	1 1
1 1	32·8		28·4	3 1
2 0	27·9	28·0 ± 0·2	28·0	4 0
2 1	23·0			
		22·1 ± 0·2	21·9	0 2
0 2	20·3			
$\Sigma(d_{fit} - d_{obs})^2$/Å^2	0·82		0·05	

As we have mentioned, ribbon-like aggregates have been reported to pack on hexagonal [8,19], oblique [9,17,19], primitive rectangular [5,6,13,31] and centred rectangular lattices [7,16,18,19,32]. The system presently under study constitutes another centred rectangular ribbon phase. It is of interest to investigate the driving force behind the formation of the different ribbon phases. We therefore review the reported experimental evidence for each type of ribbon phase to obtain further insight into this problem.

3.3. *The hexagonal ribbon phase*

Hendrikx and Charvolin [8] have, on the basis of SANS measurements, suggested that the aggregates are ribbon-like in parts of the hexagonal phase of the sodium decyl sulphate/1-decanol/water system. This observation is supported by their SAXS measurements, since if the aggregates cross-sections are assumed to be circular, their radius would have to be greater than the fully stretched surfactant chain length [8], and would thus violate the alkyl chain packing constraint. This argument also holds for the rods of the hexagonal regions close to the rectangular phase in the CTAB/water [19] and dodecyl-1,3-propylene-diamine/HCl/water [29] systems. There is then a striking similarity between the transition from a micellar solution phase to a hexagonal phase, and the transition from a hexagonal phase to a lamellar phase. The hexagonal rods grow to ribbons before a lamellar phase is formed, just as spherical micelles become elongated before a hexagonal phase is formed [28]. Moreover, a cubic phase with prolate micelles sometimes occurs intermediate between the micellar prolate phase and the hexagonal phase [10], in the same way as an intermediate ribbon phase can be formed between the hexagonal ribbon phase and the lamellar phase (one difference is the fact that other intermediate phases can sometimes be found between the hexagonal and lamellar phases).

In view of the similarities between the micellar–hexagonal and the hexagonal–lamellar phase transitions just described, it would seem reasonable to assume that the more surfactant-rich parts of the hexagonal phases of different systems, are in general, of the ribbon type.

Table 4. Observed scattering vectors, Q_{obs}, and calculated for oblique symmetry, Q_O, as presented in [9]. The unit cell dimensions, $a = 48{\cdot}8$ Å, $b = 39{\cdot}3$ Å and $\beta = 114{\cdot}1°$ (cf., figure 1 (*c*)) were used for this case. Q_R is the result from a centred rectangular fit to the data, with unit cell dimensions $a = 89{\cdot}0$ Å and $b = 39{\cdot}3$ Å (cf. figure 1 (*d*)). The composition of the sample was ~60 per cent SDS in D_2O and the temperature was 55°C. The relationship between the scattering vectors, Q, and the Bragg distances, d, is: $d = 2\pi/Q$.

hk_O	Q_O/Å^{-1}	Q_{obs}/Å^{-1}	Q_R/Å^{-1}	hk_R
1 0	0·1410	0·1411	0·1412	2 0
0 1	0·1752	0·1751	0·1748	1 1
1 1	0·2660	0·2664	0·2654	3 1
2 0	0·2820	0·2814	0·2824	4 0
1 −2	0·3198	0·3188	0·3198	0 2
2 −2	0·3487	0·3495	0·3495	2 2
0 2	0·3504			
3 0	0·4230	0·4240	0·4236	6 0
3 −2	0·4250			
$\Sigma(Q_{fit}-Q_{obs})^2$/Å^{-2}	$3{\cdot}2 \times 10^{-6}$		$3{\cdot}3 \times 10^{-6}$	

3.4. *The oblique ribbon phase*

An oblique phase (or two dimensional monoclinic phase) with elongated rods has been proposed to exist in the SDS/water system [9, 17, 20, 21]. However, recently Auvray *et al.* [18] performed SAXS measurements of high quality on this phase, and a centred rectangular structure was fitted to the data. Our calculations (see table 4) show that a centred rectangular lattice can be fitted also to Kékicheffs and Cabanes data [9] on the SDS/water ribbon phase. Auvray *et al.* suggested that the ribbon phase of the CTAB/water system is of an oblique symmetry, but also showed that a centred rectangular lattice can be fitted to their SAXS data [19]. Thus, there is to our knowledge no convincing experimental evidence in favour of the existence of an oblique ribbon phase published so far.

3.5. *The rectangular ribbon phases*

There seems little doubt that there exists a rectangular phase with ribbon-like aggregates between the hexagonal and lamellar phases. Whether the phase symmetry is primitive or centred is not yet clear, and possibly ribbon phases of both symmetries exist. In order to investigate this matter we present in table 2 the symmetries that are proposed for different rectangular ribbon phases, as based on scattering experiments. The abbreviations for the different components are explained in table 1. For the cases where the scattering data are published, we have tried to fit both centred (cmm) and primitive (pmm) rectangular lattices (according to equation (1)) to the data, and the results are displayed in table 2. While some of the data sets do not contain enough information to distinguish between the pmm and cmm symmetries, only a centred rectangular lattice can be fitted to some data sets (see tables 3 and 5 for examples). Indeed, there is no data set that favours the pmm lattice over the cmm one. Thus, the scattering data presented here taken together favour a centred rectangular ribbon phase. Several authors have studied the potassium palmitate/potassium laurate/water system, in which a ribbon phase is reported to exist [12, 33–36]. The symmetry of the phase is, according to SAXS measurements, proposed to be primitive rectangular of

Table 5. Observed Bragg spacings (d_{obs}) at 20°C for a sample that consists of 64·0 wt% potassium oleate in water [5, 6]. The results from the best primitive rectangular (pmm), d_p (unit cell dimensions $a = 53{\cdot}9$ Å and $b = 41{\cdot}9$ Å) and centred rectangular (cmm), d_c (unit cell dimensions $a = 107{\cdot}8$ Å and $b = 45{\cdot}5$ Å) fits to the data are shown.

hk_p	d_p/Å	d_{obs}/Å	d_c/Å	hk_c
1 0	53·9	53·9	53·9	2 0
0 1	41·9	41·9	41·9	1 1
1 1	33·1		28·2	3 1
2 0	27·0	27·0	27·0	4 0
2 1	22·8		22·8	0 2
0 2	21·0	21·0	21·0	2 2
$\Sigma(d_{fit}-d_{obs})^2$/Å^2	0·004		0·004	

space group pmm [37, 38]. However, no single phase rectangular sample has been X-rayed, and thus the reflections from the ribbon phase are superimposed on reflections from the coexisting phase or phases, making the data difficult to interpret. Another published piece of evidence in favour of a primitive rectangular ribbon phase is a sweep electron microscopy investigation on the potassum oleate/water system, performed by Balmbra *et al.* [13]. However, such a study on this system by Eins [39] shows a centred rectangular structure.

To conclude, it would appear that the ribbon-like aggregates prefer to pack on a centred rectangular lattice (if not on a hexagonal lattice). In the next section we investigate whether this observation can be rationalized thermodynamically.

3.6. *Theoretical aspects on the symmetry of the ribbon phases*

In order to understand the occurrence of ribbon phases, we start this section with a discussion concerning some general features of the phase behaviour of surfactant/water systems. When a charged surfactant with a single hydrocarbon tail and water are mixed together, phases consisting of spheres, infinite cylindrical rods, or infinite lamellae are commonly obtained. Due to packing constraints (i.e. the limited length of the hydrocarbon tail), the surfactant headgroup areas, A_{sp}, are roughly 75 Å^2, 50 Å^2 and 25 Å^2, respectively, for these aggregate shapes [40]. A small head group area provides a small hydrocarbon/water contact area, but also leads to a high electrostatic repulsion between the charged head groups of the surfactants. The aggregate structure that provides the best compromise between these factors is that actually obtained (other factors may affect the situation more or less). Whereas the surface energy of the system is essentially proportional to the hydrocarbon/water contact area, the electrostatic energy is strongly dependent on the number ratio of counter ions to water molecules in the system. The less water in the system, the more efficient screening of the electrostatic potential of the aggregate surfaces can be provided by the counter ions. Therefore the sequence, micellar phase–hexagonal phase–lamellar phase, is very often obtained as the surfactant concentration is increased in binary surfactant/water systems [2]. However, the stepwise decrease of A_{sp} with the surfactant concentration just given is in contradiction to the continuous increase of the counter ion/water ratio as the surfactant concentration is increased. In order to provide a smoother decrease of A_{sp} with the surfactant concentration, the aggregate radius may be somewhat bigger in the more surfactant-rich parts of each phase, than in its most water-rich parts [2, 41]. Another way to provide a smoother decrease in A_{sp} is to form aggregates with other

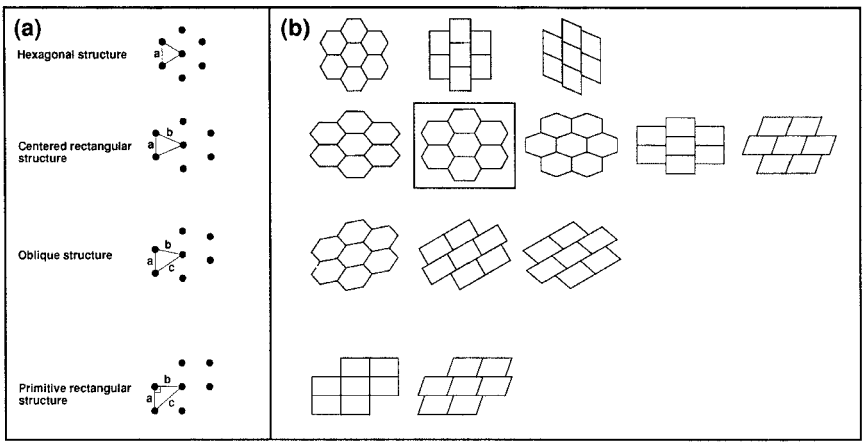

Figure 3. (*a*) The deformation of the hexagonal lattice to a centred rectangular lattice and further to oblique and primitive rectangular lattices. (*b*) Examples of cell models of these structures.

symmetries than the three discussed so far. For example, spherical micelles may grow to prolate micelles and form a solution phase [28] as well as discrete cubic phases [25], before the hexagonal phase is formed. For the same reasons intermediate phases are found between the phases consisting of infinite cylindrical rods and infinite lamellae, for example, several different bicontinuous cubic phases, the tetragonal and the rhomboh-edral phases belong to this group, as well as the ribbon phases—the object of this paper.

By deforming the cylindrical cross-section of the infinite rods, the surface to volume ratio of an aggregate with fixed smallest dimension is decreased (and thus A_{sp}). This deformation is completely analogous to the deformation of spherical micelles into prolate micelles. In view of the discussion in the section on the hexagonal ribbon phase it is evident that the deformed elongated aggregates may stay packed on a hexagonal lattice, just as a solution phase may consist of prolate micelles. However, ribbon phases with lower than hexagonal symmetry are also obtained and we continue by discussing these from a thermodynamic point of view.

The deformation of the hexagonal lattice into lattices of lower symmetry pertaining to ribbon phases is shown in figure 3 (*a*). The hexagonal lattice can be divided into equilateral triangles with sides of length *a*. A deformation to a centred rectangular symmetry with isosceles triangles, with sides of length *a* and *b*, is obtained by stretching the hexagonal lattice in one direction. This lattice can be further deformed by shearing the layers with respect to each other, a procedure that results in different oblique structures, all of which have triangles with sides of different lengths (*a*, *b*, and *c*). Finally, a primitive rectangular lattice is obtained when one of the angles is 90°.

To investigate the free energy of surfactant systems it is fruitful to use an approach based on a cell model [4, 42]. The volume of the system is then divided in cells of equal size with the condition that the shape of the cells should be such that the whole volume is filled when one cell is centred at every point in the lattice. One aggregate of a certain shape (not necessarily the same as that chosen for the cell) is then placed in every cell. When the cell model is applied to phases with elongated rods of either cylindrical or ribbon-like cross-sections, the simplest cell geometries would be those where the shape of the cells is approximated by hexagons or by parallellograms. The resulting structures

of the hexagonal, rectangular, and oblique phases are then typically modelled as in figure 3(*b*). This procedure leaves us with an infinite number of cell geometries. Moreover, the shape of the aggregates is not specified by the geometry of the cell. Clearly, this situation does not suffice to specify the phase structure and we would then ask the question as to whether some particular choice of geometry for the cells and the aggregates is more favourable for a system with ribbon-like aggregates, with regard to the Gibbs free energy of the system, than others. Today our theoretical knowledge of these complicated systems is not sufficient to perform such calculations in detail, but we can consider the most important contributions to the energy of the system.

Experimental and theoretical results show that it is energetically advantageous to maintain a constant thickness of the water layer between the neighbouring aggregates [4], and to form simultaneously aggregates where the interfacial area is at a minimum (and with the added constraint that there are no head groups in the interior of the aggregates) [4]. These are general conditions, and we now investigate for which cell and aggregate geometries these two conditions are best fulfilled for a system with ribbon-like aggregates. In doing so we start by considering the aggregate geometry. We approximate the aggregate shape with that of a hexagon with as yet unspecified angles and side lengths. The choice of a hexagonal shape is dictated by the fact that this geometry is simple to treat and yet contains the main features of the real aggregates. The actual shape of the aggregate does, not of course, contain any corners but is of smooth and complicated geometry.

In order to obtain the hexagon or parallelogram where the interface area is at a minimum we perform the following calculation. Let us fix the cross-sectional area of the aggregate, A_{cs}, to a certain value, and let the smallest dimension of the aggregate, r_s (cf. figure 6), be given by some length of the surfactant (not necessarily the all-*trans* length of the chain). We have calculated the envelope surface of the aggregates for different aggregational shapes (that is, by varying α, β, and γ in figure 4), with the constraints of fixed values for r_s and A_{cs}. Not surprisingly, it turns out that the envelope surface of the aggregate has its minimum value when $\alpha = 0°$, $\beta = 30°$ and $\gamma = 120°$. This result is independent of the chosen values for r_s and A_{cs}, and so holds for all systems with deformed aggregates that are approximated by hexagons. Thus we assign the value 120° to all six angles of the hexagon representing the aggregate. The next step is to choose a geometry for the cell.

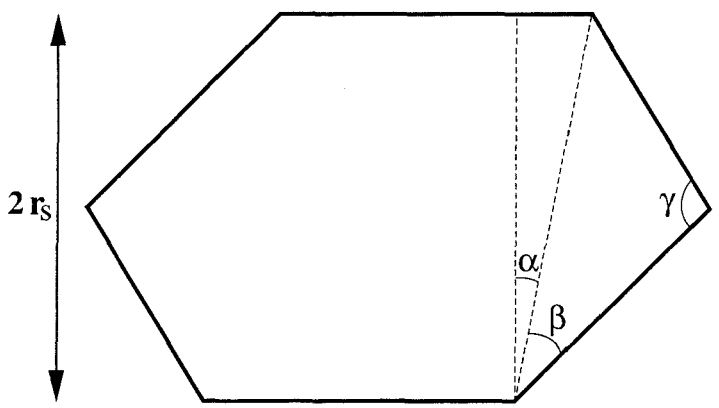

Figure 4. The circumference of the hexagon with fixed r_s and A_{cs} has its minimum value for $\alpha = 0°$, $\beta = 30°$ and $\gamma = 120°$.

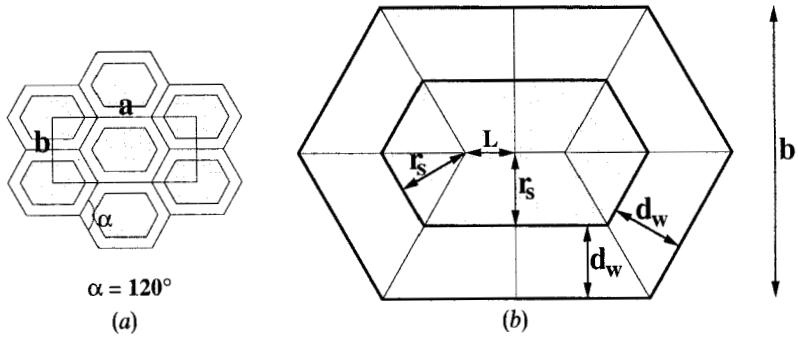

Figure 5. An illustration of the hexagon-rod model with the dimensions used indicated.

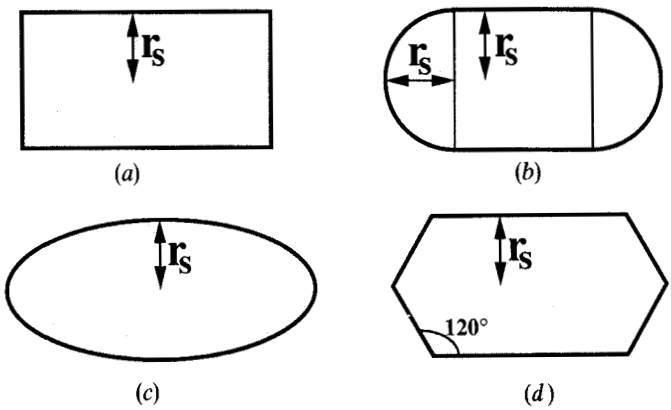

Figure 6. The approximations of the aggregate cross sections in (*a*) the rectangular-rod model, (*b*) the ribbon-rod model, (*c*) the elliptic-rod model and (*d*) the hexagon-rod model.

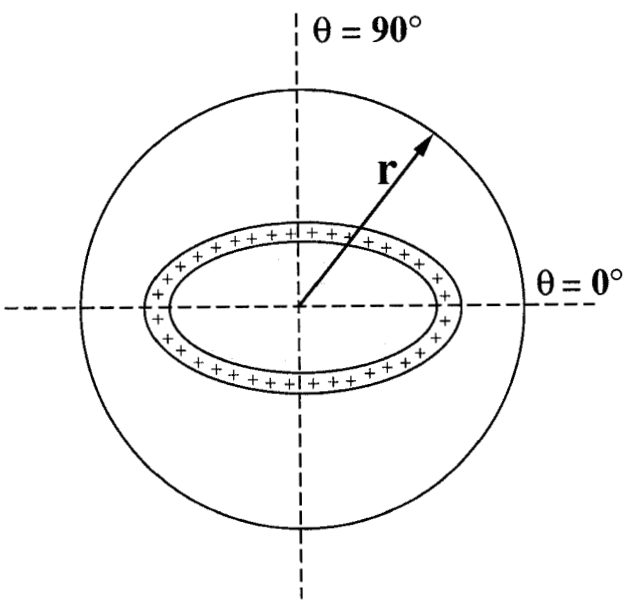

Figure 7. The origin of the electric quadrupole moment outside a charged rod with a non-circular cross-section.

As we have noted it is energetically favourable for a surfactant system to maintain a constant value of the inter-aggregate distance [4, 40]; an example of this is a lamellar phase. We assume, therefore, that the water layer thickness will be constant between the aggregates and this criterion determines the geometry of the cell. With this condition the cell geometry will have to be a hexagon with the same angles as those of the aggregate, i.e. 120°, as in the cell model which is framed in figure 3 (*b*). We note in passing that the geometries of the cell and the aggregates thus arrived at ensures that the water layer thickness between the aggregates is at its maximum value. For all oblique and primitive rectangular cell models, as well as for all centred rectangular cell models for which not all cell and aggregate angles equal 120°, the conditions of constant water layer thickness and small interfacial area of the aggregates are less well satisfied.

In conclusion, the arguments presented here lead to a phase structure as that presented in figure 5 (*a*), for which all cell and aggregate angles are 120° and the water layer thickness is constant. The lattice of this structure has a centred rectangular symmetry of space group cmm, in agreement with the experimental results for a number of ribbon phases (cf. table 2). In what follows we will term the specific structural model of figure 5 the hexagon-rod model.

3.7. *The space group of the rectangular ribbon phase*

The previous theoretical reasoning, indicates that the ribbon-like aggregates pack on a centred rectangular lattice of symmetry cmm. However, the discussion is based on the simple, but important, arguments that the water layer thickness between the aggregates should be constant and that the aggregate interfacial area should be at a minimum (under given constraints). Even though these principals are certainly important, other factors may also contribute, and thus it is conceivable that some ribbon systems may have differing structures. An example is the formation of the hexagonal ribbon phase [8], for which both these conditions cannot be fulfilled simultaneously. One reason why this phase is formed is that it is entropically favoured as compared to the rectangular ribbon phases. This follows since both the degree and the orientation of the deformation of the hexagonal ribbons may vary in time as well as spatially along the rods.

Another example is given by structures of space group pgg (see figure 1 (*b*)). This structure has been suggested to exist by Alpérine *et al.* [16]. One factor, suggested by these workers, that may contribute to the formation of this structure, is the fact that the deformed aggregates have an electric quadrupolar moment which may cause the aggregates to pack in a different manner. The electrostatic potential, Φ, will in addition to its dependence upon r, also be a function of θ, $\Phi(r, \theta)$ (see figure 7). It might then be energetically advantageous for the system to orient the quadrupoles (i.e. the aggregates) with respect to each other, even though the water layer thickness between the aggregates must then necessarily vary.

The system that was studied by Alpérine *et al.* [16] is the SdS/decanol/water system (unfortunately, as far as we are aware, the SAXS data set has not been published). A conclusion, based on SANS data, reached by these workers is that the decanol fraction is higher at the central parts of the SdS/decanol aggregates than at the edges [16]. As noted by Alpérine *et al.* this means that the electrostatic potential decreases at the central parts of the aggregate as compared to the edges, when decanol is introduced into the system. The aggregates then act as stronger electric quadrupoles than would otherwise be the case, and the formation of a rectangular phase of space group pgg may

then be favoured on behalf of space group cmm. It should be noted that unit cells of symmetry pgg could be fitted to all scattering data of table 2. This follows since the pgg and cmm unit cells may have the same dimensions. However, the pgg lattice is of lower symmetry than the cmm lattice, and therefore more Bragg reflections are allowed for the pgg-case than for the cmm-case (see equation (1)). In no case of the systems studied in table 2 have any of these additional allowed lines been reported, a fact that favours the cmm symmetry. To conclude, further experimental studies would be required to settle this matter.

3.8. *The axial ratio of the ribbon-like aggregates from SAXS and the hexagon-rod model*

The cross-sectional area of the aggregates can be obtained from the aggregate volume fraction, together with the unit cell dimensions as obtained from SAXS or SANS measurements. This information is, however, not sufficient to determine the dimensions of the aggregates, and so we need to involve a model to obtain for instance the axial ratio of the aggregates. In available models for the ribbon phase, the cross-section aggregates of the has been approximated by rectangles [6, 31], hemi-circular capped rectangles [9, 12, 34, 35, 43], and ellipses [32, 44] (see figure 6). Regardless of the aggregate shape that is chosen, we can determine its dimensions by assuming a value of the length of the smallest dimension of the aggregate (r_s). For example, in the approximation with hemi-circular capped rectangles, r_s has been assumed to be the mean value of the radius of the hexagonal and the lamellar aggregates in the same system [9, 43]. Different approaches have been used for the rectangular approximation. Luzzati and co-workers [6] assumed the dimensions of the rectangles to be proportional to the cell dimensions, whereas Ekwall *et al.* [31] calculated the dimensions of the rectangles by assuming the interaggregate water layer to have a constant thickness. In view of the discussion in the previous theoretical section, the last model leads to a physically reasonable packing of the aggregates. On the other hand, hemi-circular capped rectangles or ellipses would appear to be better approximations to the internal structure of the aggregates, but they do not give rise to a constant water layer thickness between the aggregates.

The hexagon-rod model presented here considers both the internal aggregate structure and the inter-aggregate interactions of the phase, and we shall use it to calculate the dimensions of the aggregates of the centred rectangular ribbon phase of symmetry cmm. In figure 5 (*b*), a detailed picture of the cell of the hexagon-rod model is displayed. Once the rectangular unit cell dimensions (a and b) are obtained, the dimensions of the hexagon-rod model cell are given. Then the length of the lamellar-like part of the aggregate is $2L = 1/2(a - b\sqrt{3})$ and the smallest aggregate dimension is

$$r_s = -L/\sqrt{3} + \sqrt{[(ab\phi\sqrt{3}/12 + L^2/3)]}, \tag{2}$$

where ϕ is the aggregate volume fraction. The axial ratio is defined as

$$\rho = 1 + L/r_s, \tag{3}$$

($\rho > 1$). With this definition ρ equals one for a rod with the cross-section of a regular hexagon, which corresponds to the hexagon-rod model approximation for a circular cylindrical aggregate. In order to calculate axial ratios of the deformed aggregates of the rectangular phase in different systems, we require a procedure to compute the aggregate volume fraction of the samples.

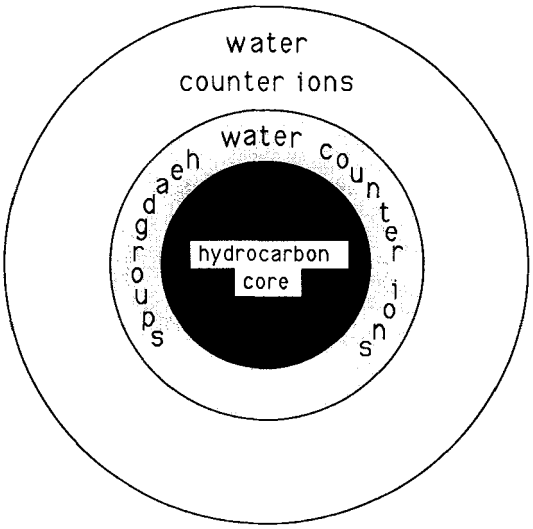

Figure 8. The hydrocarbon volume fraction of a surfactant system. Outside the hydrocarbon core there is a palisade layer with surfactant head groups, water molecules and counter ions. The rest of the cell contains counter ions and water.

3.9. *The hydrocarbon volume fraction*

To obtain information on the structure of the aggregates from SAXS data, we need to know the aggregate volume fraction of the system. Commonly the aggregate volume fraction is calculated by considering the aggregates to consist of both the amphiphilic molecules and the counter ions, and the surrounding solution to be of pure water. However, outside the homogeneous hydrocarbon core of the aggregates there is a palisade layer of mixed surfactant head groups, counter ions and water molecules. This layer is, in turn, surrounded by a mixture of water molecules and counter ions (see figure 8). We therefore use the volume fraction of the more well-defined hydrocarbon core of the aggregates (ϕ_{hc}) to calculate the aggregate structure. For any system including a surfactant (s), a cosurfactant (c) and water (w), ϕ_{hc} can be calculated according to

$$\phi_{hc}=\frac{V_{s,hc}+(n_c/n_s)V_{c,hc}}{V_s+(n_c/n_s)V_c+(n_w/n_s)V_w}, \tag{4}$$

where n_x/n_s is the number of molecules x per surfactant molecule in the sample, V_x is the volume of molecule x and $V_{x,hc}$ denotes the volume of the hydrocarbon part of molecule x. This equation is also valid when no cosurfactant is added ($n_c=0$).

3.10. *The axial ratio of the ribbon-like aggregates from NMR and the hexagon-rod model*

The line shape of the NMR spectra can be used to identify the presence of non-circular rods. The signal from deuterium labelled surfactants is particularly suited for this purpose. In addition, the axial ratio of the aggregates can be obtained from the line shape, provided that a model is chosen for the cross-section of the rods. Two such models have been presented in the literature, viz. the elliptic-rod model [32, 44] and the ribbon-rod model [12, 34, 35]. In what follows, we derive the necessary relations to obtain the axial ratio from the ^{2}H NMR line shape in terms of the hexagon-rod model. In doing so, we follow closely the lucid treatment of the analogous derivation for the

elliptic-rod model by Quist *et al.* [44]. According to [44] the asymmetry parameter, η_R, and the residual anisotropy, A_R, is given by

$$\eta_R = \frac{\langle A_N \sin^2 \theta_{RN} \cos 2\phi_R \rangle}{\langle A_N \cos^2 \theta_{RN} \rangle - \frac{1}{3}\langle A_N \rangle}, \tag{5}$$

$$A_R = \tfrac{1}{2}[3\langle A_N \cos^2 \theta_{RN} \rangle - \langle A_N \rangle], \tag{6}$$

where A_N is the local residual anisotropy, and the Euler angles θ_{RN} and ϕ_R are defined in figure 9. In this figure x_R, y_R, and z_R are the principal axes of the motionally averaged electric field gradient tensor and the z_R axis is defined by the largest component of this tensor. For a circular cylinder the z_R axis coincides with the cylinder axis, whereas the direction of the z_R axis coincides with the normal to the surface (z_N) for a lamella. As a consequence, the z_R axis changes direction for a critical value of the eccentricity of the cross-section of the elongated aggregate (see figure 9). We can, therefore, identify two regimes for the deformation, one small deformation regime where z_R is along the cylinder axis, and one large deformation regime where z_R is the normal to the most lamellar-like region of the aggregate.

The local residual anisotropy, A_N, may for a given position on the surfactant be a function of the aggregate curvature, due for instance to different packing conditions for the surfactants. However, there is experimental evidence from a number of systems that such variations are relatively small [14, 22, 32] and it is a reasonable assumption that A_N is constant over the aggregate surface, and so equations (5) and (6) are reduced to

$$\eta_R = \frac{\langle \sin^2 \theta_{RN} \cos 2\phi_R \rangle}{\langle \cos^2 \theta_{RN} \rangle - \frac{1}{3}}, \tag{7}$$

and

$$A_R = \tfrac{1}{2} A_N [3\langle \cos^2 \theta_{RN} \rangle - 1]. \tag{8}$$

In the small deformation regime, θ_{RN} is everywhere 90°, and equations (7) and (8) reduces therefore to

$$\eta_{R,SDR} = -3\langle \cos 2\phi_R \rangle, \tag{9}$$

and

$$A_{R,SDR} = -A_N/2. \tag{10}$$

At the top and the bottom of the hexagon, $\cos 2\phi_R = -1 (\phi_R = 90°, 270°)$, whereas $\cos 2\phi_R = 1/2$ at the edges (cf. figure 9) of the hexagon ($\phi_R = 30°, 150°, 210°, 330°$). Therefore, $\langle \cos 2\phi_R \rangle = 1/2 P_e - (1 - P_e) = 3/2 P_e - 1$, where P_e is the number fraction of surfactant molecules located at the edges of the hexagon, and after insertion of this expression into equation (9) we obtain

$$\eta_{R,SDR} = 3 - \tfrac{9}{2} P_e. \tag{11}$$

In the large deformation regime ϕ_R is everywhere equal to 0°, and according to equation (8)

$$\langle \cos^2 \theta_{RN} \rangle = \tfrac{1}{3}(1 + 2A_R/A_N), \tag{12}$$

and as a consequence

$$\langle \sin^2 \theta_{RN} \rangle = \tfrac{2}{3}(1 - A_R/A_N). \tag{13}$$

Insertion of equations (12) and (13) into equation (7) and with $\cos 2\phi_R = 1$, gives

$$\eta_{R,LDR} = A_N/A_R - 1. \tag{14}$$

At the top and the bottom of the hexagon, $\cos^2\theta_{RN} = 1(\theta_{RN} = 0°, 180°)$, whereas $\cos^2\theta_{RN} = 1/4$ at the edges of the hexagon ($\phi_R = 60°, 120°, 240°, 300°$). After insertion of these values into equation (8) we obtain

$$A_{R,LDR} = A_N(1 - \tfrac{9}{8}P_e), \tag{15}$$

and with this result inserted into equation (14) we finally obtain

$$\eta_{R,LDR} = (1 - \tfrac{9}{8}P_e)^{-1} - 1. \tag{16}$$

In order to derive an expression for P_e we have to make an assumption about the distribution of the surfactants on the surface of the hexagon. In the simplest approximation, the surfactants are evenly distributed over the surface, i.e. A_{sp} is constant. It might, however, be argued that A_{sp} should be smaller at the central parts of the aggregates than in other parts, since A_{sp} is typically 25 Å^2 for a lamella and 50 Å^2 for a cylindrical rod [2, 40]. We derive expressions for P_e for both of these surfactant distributions. The length of the lamellar-like region of the aggregate is $2L$ (see figures 5 and 9) in the hexagon-rod model. For the case of uniformly distributed surfactants. P_e^u is the length fraction of the aggregates' circumference which consists of edges, that is, $4(2r_s/\sqrt{3})/[6(2r_s/\sqrt{3}) + 4L]$. With the axial ratio of the aggregate as given in equation (3) we obtain

$$P_e^u = 2[3 + \sqrt{3}(\rho - 1)]^{-1}. \tag{17}$$

For the case of surfactants non-uniformly distributed over the surface, the lamellar part has to be doubly weighted, and $P_e^n = 4(2r_s/\sqrt{3})/[6(2r_s/\sqrt{3}) + 2(4L)]$, or after insertion of equation (3)

$$P_e^n = 2[3 + 2\sqrt{3}(\rho - 1)]^{-1}. \tag{18}$$

For the uniform surfactant distribution, insertion of equation (17) into equations (11), (16), (10) and (15) gives

$$\eta_{R,SDR}^u = 3 - 9[3 + \sqrt{3}(\rho - 1)]^{-1}, \qquad 1 \leqslant \rho < 1 + \sqrt{3}/2, \tag{19}$$

$$\eta_{R,LDR}^u = 9[3 + 4\sqrt{3}(\rho - 1)]^{-1}, \qquad \rho > 1 + \sqrt{3}/2, \tag{20}$$

$$A_{R,SDR}^u = -A_N/2, \qquad 1 \leqslant \rho < 1 + \sqrt{3}/2, \tag{21}$$

$$A_{R,LDR}^u = A_N(1 - \tfrac{9}{4}[3 + \sqrt{3}(\rho - 1)]^{-1}), \qquad \rho > 1 + \sqrt{3}/2, \tag{22}$$

respectively, and insertion of equation (18) into equations (11), (16), (10) and (15) respectively for the non-uniform distribution gives

$$\eta_{R,SDR}^n = 3 - 9[3 + 2\sqrt{3}(\rho - 1)]^{-1}, \qquad 1 \leqslant \rho < 1 + \sqrt{3}/4, \tag{23}$$

$$\eta_{R,LDR}^n = 9[3 + 8\sqrt{3}(\rho - 1)]^{-1}, \qquad \rho > 1 + \sqrt{3}/4, \tag{24}$$

$$A_{R,SDR}^n = -A_N/2, \qquad 1 \leqslant \rho < 1 + \sqrt{3}/4, \tag{25}$$

$$A_{R,LDR}^n = A_N(1 - \tfrac{9}{4}[3 + 2\sqrt{3}(\rho - 1)]^{-1}), \qquad \rho > 1 + \sqrt{3}/4. \tag{26}$$

The results of equations (19)–(26) are summarized in figure 10, which shows η_R and $|A_R|/|A_N|$ as functions of the hexagon axial ratio.

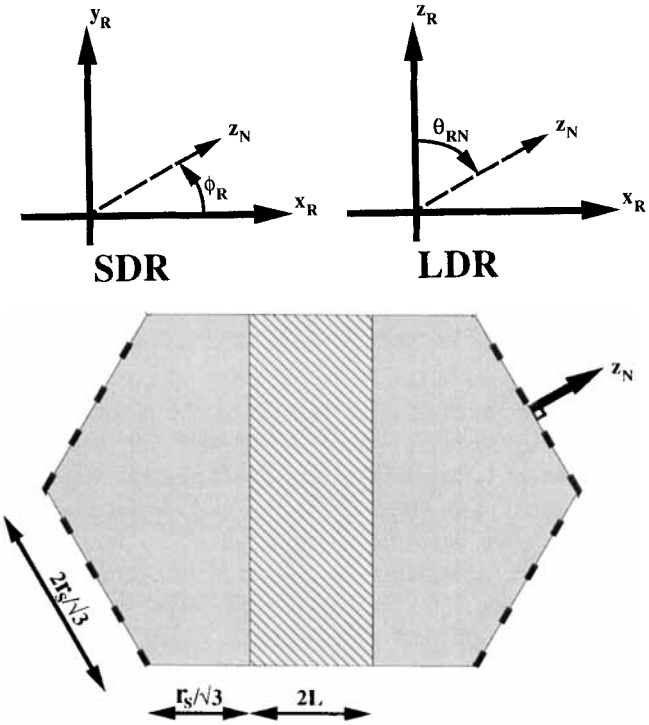

Figure 9. The Euler angles θ_{RN} and ϕ_R in the small deformation (SDR) and the large deformation regime (LDR) for the hexagon-rod model. The lamellar-like region of the hexagon is hatched and the regular hexagon-like regions are shaded. The edges of the aggregate are indicated by dashed lines.

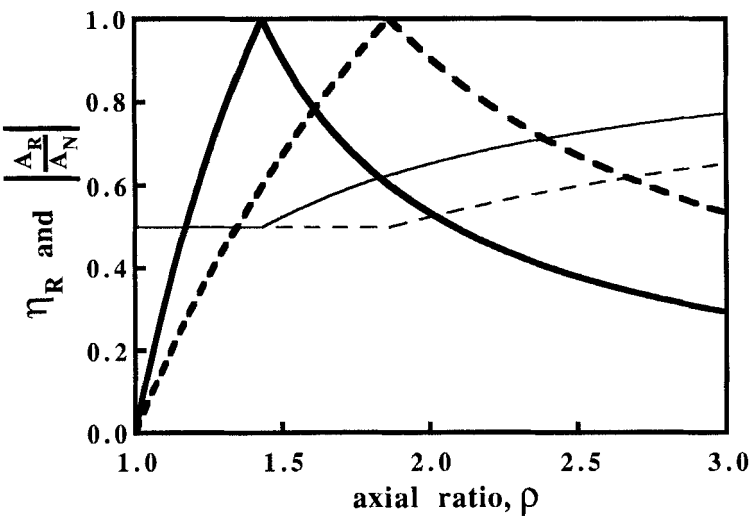

Figure 10. The asymmetry parameter, η_R (bold lines), and the residual anisotropy, A_R, as a function of the axial ratio in the hexagon-rod model. The dashed lines are for the uniform surfactant distribution and the solid lines for the non-uniform surfactant distribution (see text for details).

3.11. *Calculation of axial ratios for rectangular ribbon phases in different systems*

We have used the hexagon-rod model to calculate the axial ratio of the hydrocarbon core of the ribbon-like aggregates from the SAXS data. All of the ribbon phases of table 2 have been assumed to be of centred rectangular symmetry of space group cmm, even if the experimental evidences are not sufficient to determine this. The molecular volumes used in the calculations for the species of the different systems at various temperatures are given in table 6. The resulting axial ratios of the hydrocarbon cores are in the range 1·3 : 1 to 2 : 1. The axial ratio for the whole aggregate will have somewhat smaller values than for the hydrocarbon cores, since r_s increases on inserting surfactant head groups in the aggregates while L is constant, and $\rho = 1 + L/r_s$. For example, with a length for the head group of the trimethylammonium group of 2 Å added uniformly outside the hydrocarbon core of the rods, the axial ratio for the DoTAC/water sample decreases from 1·39 : 1 to 1·34 : 1.

The values obtained for the axial ratios agree qualitatively with results from an analysis of the lineshape of ^{2}H NMR spectra obtained for the ribbon phase in the potassium palmitate/potassium laurate/water system [12, 34, 35, 44] and in the DoTAC/water system [32]. Due to the lack of proper SAXS data for the ribbon phase of the potassium palmitate/potassium laurate/water system, a comparison between the two techniques cannot be performed for this system. For the DoTAC/water system the situation is different, since Kang *et al.* [32] have performed both SAXS and ^{2}H NMR

Table 6. The temperature dependence of the group volumes, $\partial V/\partial T$, is calculated from a linear fit to published values of the group volumes at several temperatures (see footnotes for details). The group volumes, V, at 25°C are also given.

Group	V/Å^3	$\partial V/\partial T$/A^3 K^{-1}
$-CH_3$	54·19 (*a*)*	0·1204 (*a*)
$-CH_2-$	26·99 (*a*)*	0·01771 (*a*)
Oleyl-	506·7 (*a*)*	0·4038 (*b*)
$-SO_4Na$	67·99 (*a*)*	0·1848 (*a*)
$-N(CH_3)_3Br$	141·0 (*a*)*	0·05384 (*a*)
$-N(CH_3)_3Cl$	128·2 (*a*)*	0·05384 (*c*)
–OH	17 (*d*)	0 (*g*)
–COO–	35 (*d*)	0 (*g*)
Na^+	13·6 (*e*)	0 (*g*)
K^+	26 (*f*)	0 (*g*)
DA + *z*	458·8 + 27·74*z* (*h*)	—

* Volume as obtained from the linear fit to the data.

(*a*) From [47].

(*b*) Assumed to be equal to $\partial V/\partial T$ as calculated for the octadecyl group.

(*c*) Assumed to be equal to $\partial V/\partial T$ for $-N(CH_3)_3Br$.

(*d*) From [40].

(*e*) From [48].

(*f*) The crystal ionic radius for sodium is $r_{i,Na^+} = 0{\cdot}97$ Å and for potassium $r_{i,K^+} = 1{\cdot}33$ Å. [46], whereas the volume for Na^+ in solution, 13·6 Å^3, corresponds to a radius of $r_{s,Na^+} = 1{\cdot}48$ Å. We have assumed the radius for the potassium ion to be $r_{s,K^+} = (r_{s,Na^+}) + (r_{i,K^+} - r_{i,Na^+}) = 1{\cdot}84$ Å.

(*g*) Assumed values.

(*h*) From the present work.

measurements on the sample with a composition of 81·6 wt% surfactant. The value for η reported by Kang *et al.* [32] is 0·534, which yields axial ratios for the uniform and non-uniform surfactant distribution of 1·37 : 1 and 1·19 : 1, respectively, for the hexagon-rod model. These two surfactant distributions are extreme cases, and it is reasonable to assume the distribution of the surfactant head groups on the aggregate surface to be non-uniform, but to vary smoothly around the aggregate. For such a distribution an NMR analysis would yield a value for the hexagon-rod axial ratio intermediate between those obtained for the simpler distributions that are treated in this paper. The distribution of head groups over the surface of the hexagons can be calculated by a Poisson–Boltzmann cell model approach on the hexagon-rod model, and we will present that model in a future paper.

The axial ratio obtained from SAXS data and the hexagon-rod model for this sample is 1·39 : 1 for the hydrocarbon core, and 1·34 : 1 for the case with an added head group. The latter value is the one that should be used in a comparison with the NMR result in this case, since the ^{2}H NMR spectrum is obtained for the deuterium labelled methyl groups of the surfactant head groups. Therefore, the axial ratio as obtained from SAXS falls intermediate between the axial ratios obtained for the two extreme cases of surfactant distributions of the NMR analysis.

4. Conclusions

Ribbon phases of hexagonal, centred rectangular, primitive rectangular and oblique symmetries have been proposed to exist in surfactant systems. The main results of the present work are as follows.

(i) It is proposed that the normal hexagonal phases in surfactant systems, are in general, of the ribbon type in the more surfactant-rich regions of the phase diagrams.

(ii) Of the ribbon phases of lower than hexagonal symmetry, scattering measurements for different systems strongly favour the centred rectangular symmetry. There is, to our knowledge, no published experimental indication that favour the existence of either the oblique symmetry or the primitive rectangular symmetry.

(iii) The structure of ribbon phases is discussed from a theoretical point of view. The discussion is based on some physically reasonable assumptions concerning the internal aggregate shape and the inter-aggregate interactions, and the technique used is a cell model approach in which the aggregates as well as the cells are modelled as hexagons, or as parallelograms. The main result from this discussion is that a centred rectangular ribbon phase (of space group cmm) would be energetically favoured as compared to the primitive rectangular and oblique ribbon phases, in accord with the experimental results.

(iv) We call the cell model which represents the energetically most favoured structure in the theoretical discussion (see figure 5), the hexagon-rod model. By use of this model the aggregates dimensions can be obtained from NMR data for ribbon phases, as well as from scattering data for centred rectangular ribbon phases. The smallest dimension of the aggregates is not required as an input parameter in the calculations. Aggregate axial ratios in the range from 1·2 : 1 to 2 : 1 are obtained for the rectangular ribbon phases investigated with these models.

We thank Dr Krister Fontell for help in performing the SAXS measurements, Professor Håkan Wennerström for helpful comments, and the Swedish National Science Research Council for financial support.

References

[1] MARSDEN, S. S. J., and MCBAIN, J. W., 1948, *J. Am. chem. Soc.*, **70,** 1973.
[2] EKWALL, P., 1975, *Advances in Liquid Crystals*, Vol. 1, edited by G. H. Brown (Academic Press), p. 1.
[3] ROSS, S., and MCBAIN, J. W., 1946, *J. Am. chem. Soc.*, **68,** 296.
[4] JÖNSSON, B., and WENNERSTRÖM, H., 1987, *J. phys. Chem.*, **91,** 338.
[5] LUZZATI, V., MUSTACCHI, H., SKOULIOS, A. E., and HUSSON, F., 1960, *Acta crystallogr.*, **13,** 660.
[6] HUSSON, F., MUSTACCHI, H., and LUZZATI, V., 1960, *Acta crystallogr.*, **13,** 668.
[7] HENDRIKX, Y., and CHARVOLIN, J., 1981, *J. Phys.*, **42,** 1427.
[8] HENDRIKX, Y., and CHARVOLIN, J., 1987, *Liq. Crystals*, **3,** 265.
[9] KÉKICHEFF, P., and CABANE, B., 1987, *J. Phys., Paris*, **48,** 1571.
[10] FONTELL, K., 1990, *Colloid Polym. Sci.*, **268,** 264.
[11] ANDERSON, D. M., 1990, *J. Phys., Paris, Colloque*, **7,** 1.
[12] CHIDICHIMO, G., VAZ, N. A. P., YANIV, Z., and DOANE, J. W., 1982, *Phys. Rev. Lett.*, **49,** 1950.
[13] BALMBRA, R. R., BUCKNALL, D. A. B., and CLUNIE, J. S., 1970, *Molec. Crystals liq. Crystals*, **11,** 173.
[14] HENRIKSSON, U., BLACKMORE, E. S., TIDDY, G. J. T., and SÖDERMAN, O., 1992, *J. phys. Chem.*, **96,** 3894.
[15] VAZ, N. A. P., and DOANE, J. W., 1980, *Physics Lett.*, **77A,** 325.
[16] ALPÉRINE, S., HENDRIKX, Y., and CHARVOLIN, J., 1985, *J. Phys. Lett., Paris*, **46,** 27.
[17] WOOD, R. M., and MCDONALD, M. P., 1985, *J. chem. Soc. Faraday Trans. 1*, **81,** 273.
[18] AUVRAY, X., PERCHE, T., ANTHORE, R., PETIPAS, C., RICO, I., and LATTES, A., 1991, *Langmuir*, **7,** 2385.
[19] AUVRAY, X., PETIPAS, C., ANTHORE, R., RICO, I., and LATTES, A., 1989, *J. phys. Chem.*, **93,** 7458.
[20] LEIGH, I. D., MCDONALD, M., WOOD, R. M., TIDDY, G. J. T., and TREVETHAN, M. A., 1981, *J. chem. Soc. Faraday Trans. 1*, **77,** 2867.
[21] RENDALL, K., TIDDY, G. J. T., and TREVETHAN, M. A., 1983, *J. chem. Soc. Faraday Trans. 1*, **79,** 637.
[22] KHAN, A., FONTELL, K., LINDBLOM, G., and LINDMAN, B., 1982, *J. phys. Chem.*, **86,** 4266.
[23] KIESSIG, H., 1942, *Kolloid-Z.*, **98,** 213.
[24] FONTELL, K., 1974, *Liquid Crystals and Plastic Crystals*, Vol. 2, edited by G. W. Gray and P. A. Winsor (Ellis Horwood), Chap. 4, p. 1.
[25] FONTELL, K., FOX, K. K., and HANSSON, E., 1985, *Molec. Crystals liq. Crystals*, **1,** 9.
[26] JOHANSSON, L. B.-Å., and SÖDERMAN, O., 1987, *J. phys. Chem.*, **91,** 5275.
[27] SONIN, A. S., 1987, *Sov. Phys. Usp.*, **30,** 875.
[28] HALLE, B., LANDGREN, M., and JÖNSSON, B., 1988, *J. Phys.*, **49,** 1235.
[29] HAGSLÄTT, H., SÖDERMAN, O., and JÖNSSON, B. (to be published).
[30] 1952, *International Tables for X-ray Crystallography*, Vol. 1 (The Kynoch Press).
[31] EKWALL, P., MANDELL, L., and FONTELL, K., 1969, *J. Colloid Interface Sci.*, **31,** 508.
[32] KANG, C., SÖDERMAN, O., ERIKSSON, P. O., and STAEL VON HOLSTEIN, J., 1992, *Liq. Crystals*, **12,** 71.
[33] DOANE, J. W., CHIDICHIMO, G., and GOLEMME, A., 1984, *Molec. Crystals liq. Crystals*, **113,** 25.
[34] CHIDICHIMO, G., GOLEMME, A., and DOANE, J. W., 1985, *J. chem. Phys.*, **82,** 4369.
[35] CHIDICHIMO, G., GOLEMME, A., DOANE, J. W., and WESTERMAN, P. W., 1985, *J. chem. Phys.*, **82,** 536.
[36] RAUDINO, A., GRASSO, D., LA ROSA, C., DIPASQUALE, G., CHIDICHIMO, G., and CHECCHETTI, A., 1989, *Liq. Crystals*, **6,** 435.
[37] LIS, L. J., and QUINN, P. J., 1986, *Molec. Crystals liq. Crystals*, **140,** 319.
[38] LIS, L. J., QUINN, P. J., and COLLINS, J. M., 1989, *Molec. Crystals liq. Crystals*, **170,** 119.
[39] EINS, S., 1966, *Naturwissenschaften*, **53,** 551.

[40] JÖNSSON, B., 1981, Thesis, University of Lund.
[41] GALLOT, B., and SKOULIOS, A. E., 1968, *Kolloid-Z.*, **208,** 37.
[42] JÖNSSON, B., WENNERSTRÖM, H., and HALLE, B., 1980, *J. phys. Chem.*, **84,** 2179.
[43] KÉKICHEFF, P., and CABANE, B., 1988, *Acta crystallogr.* B, **44,** 395.
[44] QUIST, P.-O., and HALLE, B., 1988, *Molec. Phys.*, **65,** 547.
[45] BENIGNI, S., and SPIELBERG, N., 1987, *Molec. Crystals liq. Crystals* B, **150,** 301.
[46] 1971, *Handbook of Chemistry and Physics*, Vol. 52 (The Chemical Rubber Co., Ohio).
[47] REISS-HUSSON, F., and LUZZATI, V., 1964, *J. chem. Phys.*, **68,** 3504.
[48] HAYTER, J. B., and PENFOLD, J., 1983, *Colloid Polym. Sci.*, **261,** 1022.